IOP Publishing Measurement Science and Technology
Meas. Sci. Technol. 31 (2020) 035012 (8pp) https://doi.org/10.1088/1361-6501/ab502a

Parameter calibration of a vision sensor with a geometric similarity constraint

Qiyue Wang[1], Zhongyu Wang[2] and Zhendong Shang[3]

[1] Department of Science, The George Washington University, Washington, DC, 200052, United States of America
[2] School of Instrumentation Science and Opto-electronics Engineering, Beihang University, Beijing 100083, People's Republic of China
[3] School of Mechatronics Engineering, Henan University of Science and Technology, Luoyang, 471003, People's Republic of China

E-mail: wangqiyue@gwu.edu

Received 30 July 2019, revised 21 October 2019
Accepted for publication 22 October 2019
Published 31 December 2019

Abstract

The precise parameters of vision sensors determine how accurately the device obtains its results. A novel effective approach, based on geometry similar constraint, has been derived. The proposed method decouples the lens distortion coefficients and linear parameters of the camera successfully. It is also able to estimate the camera's parameters with a small number of collinear points. All the distortion coefficients are solved through a geometry similar constraint model. Then corrected images are used to estimate linear parameters once distortion coefficients are acquired. Both a computer simulation and real-life experiment are carried out to validate the performance of the proposed method. The number of collinear points is first discussed with training data, and results showed the proposed method works better compared to currently widely used methods. The proposed method is also compared with current planar target based methods, which are commonly adopted in practical experiments. The results indicate that the proposed method is more reliable and effective.

Keywords: machine vision, calibration, measurement

(Some figures may appear in colour only in the online journal)

1. Introduction

In recent years, the vision-based measuring system has been increasingly used in the field of industrial measurement, in areas such as processing, assembly, and quality inspection, etc [1]. As one of the significant technologies, the calibration of the parameters of vision sensors directly influences their measurement precision [2]. Calibration is the 3D metric information extraction of an object in the spatial World Coordinate System (WCS) from its projections on the image plane or Image Coordinate System (ICS), based on a mathematical model and geometric relationship [3].

Generally speaking, camera calibration consists of two steps. The first step involves the choice of an appropriate camera model, which can be divided into either linear or non-linear, which can be used to describe the behavior of the imaging system [4, 5]. The second step is the estimation of all parameters that a certain camera model incorporates, i.e. the interior and exterior orientation of the vision system, as well as distortion parameters [6]. The linear camera model is an ideal model, and is very easy to calibrate, thus seldom used today [4]. Non-linear camera calibration has become mainstream, in which the lens distortion model is included in the calibration process to improve the precision [7, 8].

Researchers have achieved many advances in the field, which can be classified into two categories [9, 10]. The first is auto- or self-calibration, which epipolar constraints and point correspondences between multiple views are used. Auto- or self-calibration does not need to know the 3D geometrical information of reference points [11], but the method lacks high stability [12]. The second achievement is general traditional calibration, which requires placing a calibration reference (also called targets) in front of the camera [13, 14]. The targets own multiple feature points whose 3D coordinates are exactly known. The parameters of the camera model are deduced from the relationship between the spatial coordinates

and image coordinates. Usually, 3D calibration targets are preferred, however fabricating such highly accurate 3D targets is sometimes difficult, and usually very expensive [15]. Thus, scholars try to use a 2D plane board with multiple locations to produce 3D information [16]. Zhang [17] presented a flexible technique and simple calibration method, which only requires three images of a 2D calibration template taken from different positions. This method also considered the lens distortion by involving a non-linear refinement process. Based on this, a set of optimal algorithms [18] are proposed to enhance the calibration performance by optimizing the initial camera parameters accurately. Recently, more studies have been undertaken to provide high accuracy of the calibration results. Meanwhile, other researchers have reduced the calibration errors by constructing the non-linear objective function [19].

For the above calibration methods, lens distortion parameters, as well as other intrinsic and extrinsic parameters of the camera, are estimated in a single optimization procedure at the same time [20]. Coupling among the linear and non-linear parameters can also make the calibration result rather unreliable [8]. Based on the invariances of collinear points, Liu [21] put forward a distortion correction method with a 2D checkboard. In addition to this, Moumen [22] and Zhou [23] derived distortion measurement that can be optimized by using non-linear search techniques to find the best distortion parameters. However, these methods need a lot of collinear points to achieve good performance. In terms of the projection optics, if a camera wants to obtain more collinear points in a certain view, the distance of the target needs to enlarge, which would lower the measurement accuracy and calibration result. Researchers have suggested an approach to deal with the lens distortion according to cross-ratio invariability [24], which can construct constraint function with four collinear points. It still requires a large target, though only four points are needed.

Our goal is therefore to derive an effective way to decouple the estimation process of distortion coefficients and linear parameters for the purpose of yielding more stable and reliable results. We utilize geometry similar constraint (GSC) to describe the relationship of the image points. In accordance with the GSC of a purely pin-hole model, we determine the distortion coefficients. Once the these are obtained, linear parameters are easy to calculate by linear camera equation. Furthermore, our method can estimate the parameters with a smaller number of pattern points. This means we can use a smaller target.

2. Calibration model

2.1. Imaging model

For any feature point P on the surface of a spatial object, the camera can observe the P from the world coordinates system $O_w - x_w y_w z_w$, denoted by (x_w, y_w, z_w). The arrangement of points in the image plane can be approximated by the pin-hole model [8, 17], as shown in figure 1. The point P is projected through the projection center of the lens to the point p_u at the image plane. The coordinates of p_u in the image coordinates

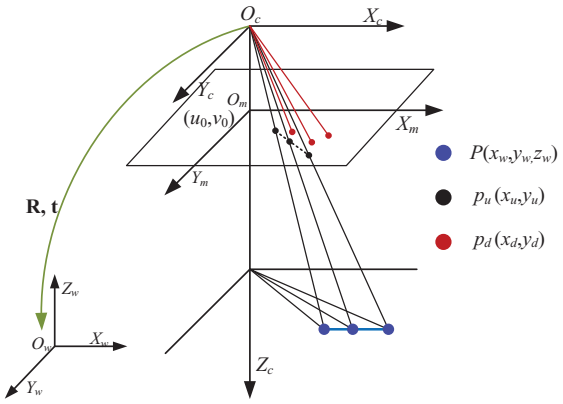

Figure 1. The imaging model of the vision sensor.

system $O_m - X_m Y_m$ are (x_u, y_u). Assume that p_d is the real distorted projection of P considering the lens distortion.

The coordinates of P in $O_w - x_w y_w z_w$ are denoted as $\mathbf{M}$, and its image coordinates in $O_m - X_m Y_m$ are $\mathbf{m}$. The math expression between $\mathbf{M}$ and $\mathbf{m}$ is given by equation (1):

$$w \begin{bmatrix} u \\ v \\ 1 \end{bmatrix} = \underbrace{\begin{bmatrix} f_x & s & u_0 \\ 0 & f_y & v_0 \\ 0 & 0 & 1 \end{bmatrix}}_{\mathbf{K}} \underbrace{\begin{bmatrix} \mathbf{r}_1 & \mathbf{r}_2 & \mathbf{r}_3 & \mathbf{t} \end{bmatrix}}_{\begin{bmatrix} \mathbf{R} & \mathbf{t} \end{bmatrix}} \begin{bmatrix} x_w \\ y_w \\ z_w \\ 1 \end{bmatrix} \tag{1}$$

where w is an arbitrary scale factor, and $\mathbf{K}$ is the intrinsic matrix which contains intrinsic parameters. When the axes X_m and Y_m are exactly perpendicular, the skew parameter s equals 0. The matrix $[\mathbf{R}\ \mathbf{t}]$ is the extrinsic parameters, and $\mathbf{r}_i$ is the ith column of $\mathbf{R}$.

2.2. Lens distortion

A real camera system usually exhibits unavoidable lens distortion. In this paper, we only consider the first two terms of radial distortion and the tangential distortion, as they are enough to describe the lens distortion in high-accuracy measurement [25]. Some more elaborate models, such as high-term radial components and prism distortion, do not really help (as this is negligible when compared with sensor quantization), but instead may cause numerical instability [16, 26, 27]. Without loss of generality, we can set the principle point as the center of distortion (COD), and the origin point of the ICS is moved to the COD. Thus, the distortion model is shown as:

$$\begin{cases} \hat{\mathbf{m}} - \mathbf{m} = \underbrace{\mathbf{m}\left(k_1\lambda^2 + k_2\lambda^4\right)}_{\text{Radial}} + \underbrace{\begin{bmatrix} 2p_1 x_u y_u + p_2(\lambda^2 + 2x_u^2) \\ p_1(\lambda^2 + 2y_u^2) + 2p_2 x_u y_u \end{bmatrix}}_{\text{Tangential}} \\ \hat{\mathbf{m}} = \begin{bmatrix} x_d \\ y_d \end{bmatrix}, \mathbf{m} = \begin{bmatrix} x_u \\ y_u \end{bmatrix}, \lambda = \left| \frac{\mathbf{m}}{f_x f_y} \right| \end{cases} \tag{2}$$

where k_1, k_2 are the radial distortion coefficients of the lens and p_1, p_2 are the tangential distortion coefficients. $\hat{\mathbf{m}}$ and $\mathbf{m}$ are the image coordinates of the real distorted point and undistorted point, respectively.

3. Methodology

3.1. Dealing with distortion

Our goal is to find the transformation that maps the actual camera image plane onto an image following the perspective camera model. The following fundamental property is often used: a camera follows the perspective model if and only if the projection of every 3D line in space onto the camera plane is a line [20, 23]. Several distortion measures can be used to find the best calibration parameters. However, most of them are based on the method of linear regression, and lack enough precision in cases with a small number of collinear points. The basic idea of GSC is to evaluate the relevancy level of geometrical similarity. Theoretically, GSC needs as a few as three points.

Suppose there are n points on a spatial straight line l, their projections to the image plane compose points set $\hat{\mathbf{L}}$, and its corresponding undistorted ideal image points set is $\mathbf{L}$, as follows:

$$\begin{aligned}\hat{\mathbf{L}} &= \left\{\hat{L}_i = \begin{bmatrix}\hat{x}\\ \hat{y}\end{bmatrix}_i, i = 1, 2, \cdots, n\right\}\\ \mathbf{L} &= \left\{L_i = \begin{bmatrix}x\\ y\end{bmatrix}_i, i = 1, 2, \cdots, n\right\}.\end{aligned} \tag{3}$$

Assume there is another line with the same number of points in the images in the meantime. Their coordinate set is

$$\begin{aligned}\hat{\mathbf{G}} &= \left\{\hat{G}_i = \begin{bmatrix}\hat{x}\\ \hat{y}\end{bmatrix}_i, i = 1, 2, \cdots, n\right\}\\ \mathbf{G} &= \left\{G_i = \begin{bmatrix}x\\ y\end{bmatrix}_i, i = 1, 2, \cdots, n\right\}.\end{aligned} \tag{4}$$

The points set, and their corresponding undistorted $\mathbf{L}$, $\mathbf{G}$ are compliant with the distortion rule in equation (2).

According to the calibration model in section 2, the projection of a straight line to the image plane remains a straight line without lens distortion. Thus, the image points set $\mathbf{L}$ can constitute a straight line on the image plane. The equation of this straight line on the image plane can be denoted as:

$$\theta_1 x + \theta_2 y + \theta_3 = 0 \tag{5}$$

where θ_i is a constant coefficient, $i = 1, 2, 3$.

We solve the initial annihilator of $\mathbf{L}$ by:

$$L^0 = \{L_i^0, i = 1, 2, \cdots n\}, \text{ with } L_i^0 = L_i - L_1. \tag{6}$$

The points in $\mathbf{L^0}$ are located on a straight line with equation:

$$\theta_1 x + \theta_2 y = 0. \tag{7}$$

Besides this we define the one-term scale of $\mathbf{L}^0$ below:

$$\mathbf{L}^1 = \left\{L_i^1, i = 1, \cdots n\right\}, \text{with } L_i^1 = \frac{L_i^0}{L_2^0}, L_1^1 = L_1^0. \tag{8}$$

We take the same operation mentioned above to deal with another line points set $\mathbf{G}$, and obtain the one-term scale set $\mathbf{G}^1$.

Table 1. The extrinsic parameters of images.

Image No	Rotation angle/°	Translation vector/mm
1	[0, 0, 20]	[−100, −100, 500]
2	[0, 20, 0]	[−120, −100, 450]
3	[20, 0, 0]	[−100, −120, 400]
4	[30, 10, 10]	[−50, −70, 450]
5	[0, 15, 10]	[−80, −100, 470]

This leads us to being able to construct the GSC function as follows:

$$\begin{cases}\eta_i = \dfrac{\min\limits_{i=1}^{n}\left|G_i^1 - L_i^1\right| + \xi\max\limits_{i=1}^{n}\left|G_i^1 - L_i^1\right|}{\left|G_i^1 - L_i^1\right| + \xi\max\limits_{i=1}^{n}\left|G_i^1 - L_i^1\right|}\\ \gamma = \frac{1}{n}\sum\limits_{i=1}^{n}\eta_i\end{cases} \tag{9}$$

where ξ is the resolution coefficient, satisfying $\xi \in [0, 1]$. Without loss of generality, we let $\xi = 0.9$ in this paper to improve accuracy. Thanks to all the points being on a straight line, the theoretical value of γ is identically equal to 1.

We also construct function based on a single straight line; the GSC of points set $\mathbf{L}$ can be given by:

$$\varepsilon = \frac{\left(\sum_{i=1}^{n-1} x_i^1 + \xi x_n^1\right)^2 + \left(\sum_{i=1}^{n-1} y_i^1 + \xi y_n^1\right)^2}{\left(\sum_{i=1}^{n-1} x_i^1 + \xi x_n^1\right)^2 + \left(\sum_{i=1}^{n-1} y_i^1 + \xi y_n^1\right)^2 + \left(\sum_{i=1}^{n-1}\left(x_i^1 - y_i^1\right) + \xi\left(x_n^1 - y_n^1\right)\right)^2}. \tag{10}$$

Thus, we can solve them simultaneously to enhance the precision.

If a camera captures one image which contains f lines, in a similar way a straight line map to γ, ε is denoted as:

$$\begin{cases}\varepsilon_i, i = 1, \cdots f\\ \gamma_b^a, a \neq b = 1, \cdots f\end{cases} \tag{11}$$

where theoretical values of elements in γ, ε are identically equal to 1 according to the straight-line invariance in the algebraic projection geometry.

To solve the distortion coefficients, an objective function $\Phi(k_1, k_2, p_1, p_2)$ is defined below:

$$\Phi(k_1, k_2, p_1, p_2) = \sum\left(\gamma_b^a - 1\right)^2 + \left(\varepsilon_i - 1\right)^2. \tag{12}$$

The distortion coefficients are solved by minimizing $\Phi(k_1, k_2, p_1, p_2)$; we leverage a non-linear optimization algorithm to acquire the results.

3.2. Linear parameters calibration

Since a planar calibration board is used, we assume the plane $x_w - o_w - y_w$ coincides with the calibration board plane. As per this assumption, we let $z_w = 0$ without loss of generality. Therefore, the third column vector $\mathbf{r_3}$ of $\mathbf{R}$ in equation (1) is omitted, and equation (1) is simplified by:

$$w\begin{bmatrix}u\\ v\\ 1\end{bmatrix} = \mathbf{K}\begin{bmatrix}\mathbf{r_1} & \mathbf{r}_2 & \mathbf{t}\end{bmatrix}\begin{bmatrix}x_w\\ y_w\\ 1\end{bmatrix}. \tag{13}$$

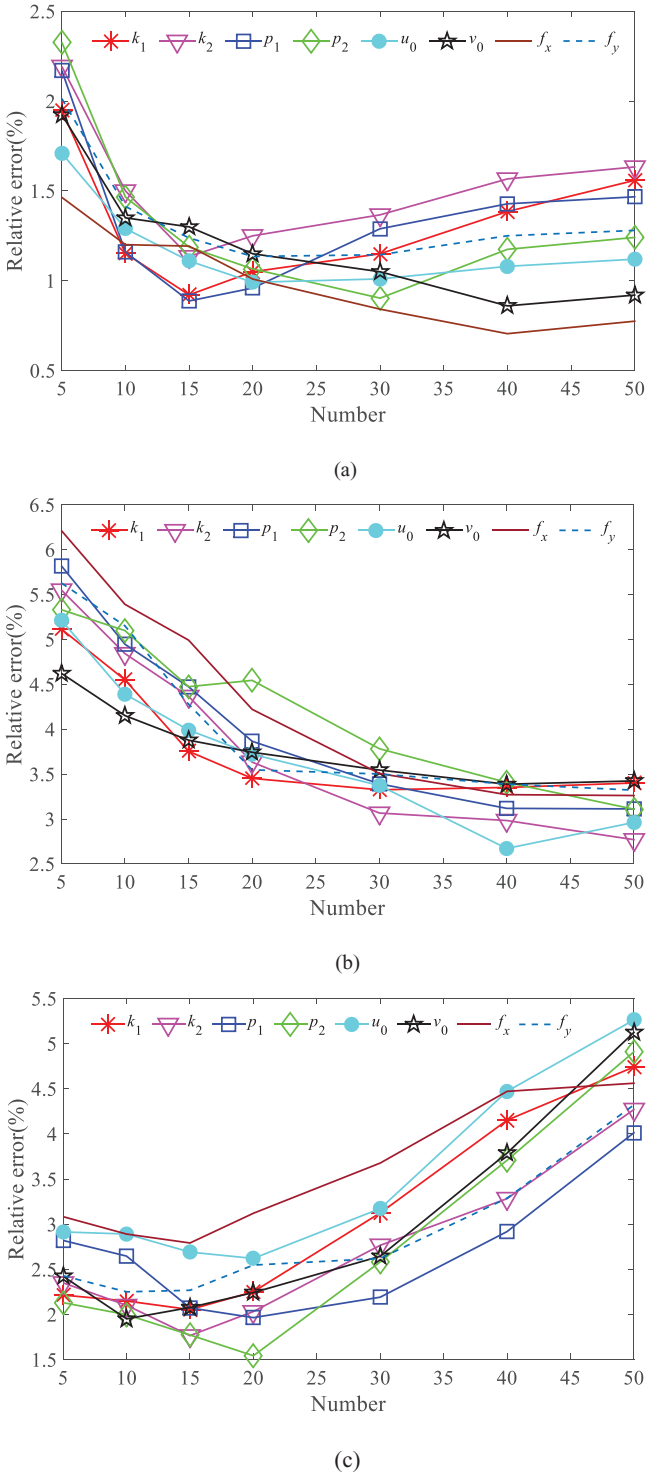

Figure 2. The relative error of camera parameters calculated by using the NCM and our proposed method. (a) Results of our proposed method, (b) results using the NCM, (c) results using the CRI.

The homographic matrix $\mathbf{H}$ describes the mapping relationship between the image plane and the object plane.

$$w\mathbf{m} = \mathbf{HM}, \mathbf{H} = \begin{bmatrix} h_1 & h_2 & h_3 \end{bmatrix} = \tau\mathbf{K}\begin{bmatrix} \mathbf{r}_1 & \mathbf{r}_2 & \mathbf{t} \end{bmatrix} \quad (14)$$

where h_i is the ith column of the homographic matrix $\mathbf{H}$, which is defined up to a scale factor.

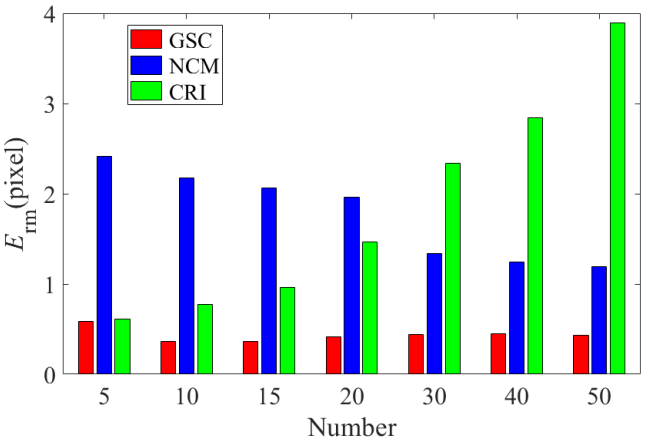

Figure 3. Mean reprojection error of different numbers of collinear points.

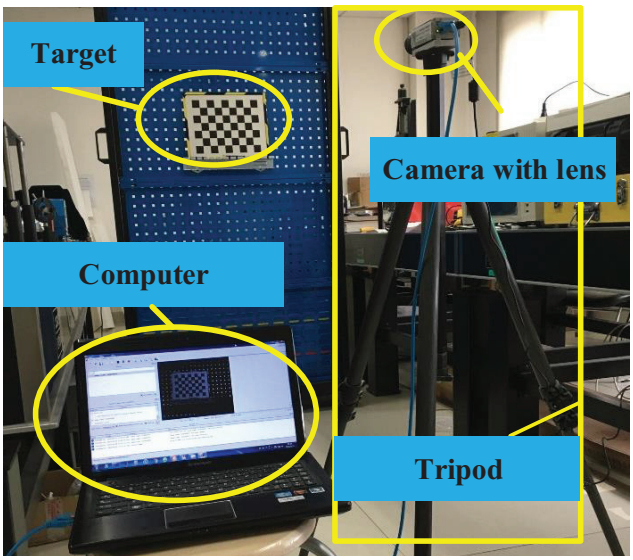

Figure 4. Camera calibration experiment system.

According to equation (14), we obtain the least squares estimation of the homographic matrix $\mathbf{H}$. We have the following two fundamental constraints for the intrinsic parameters:

$$\begin{cases} h_1^T\mathbf{K}^{-T}\mathbf{K}^{-1}h_2 = 0 \\ h_1^T\mathbf{K}^{-T}\mathbf{K}^{-1}h_1 = h_2^T\mathbf{K}^{-T}\mathbf{K}^{-1}h_2 \end{cases}. \quad (15)$$

The detailed algorithm for solving the intrinsic parameters matrix with an analytic solution after homographic estimation is in [16]. Once the intrinsic parameter matrix $\mathbf{K}$ is obtained, we get the extrinsic parameters of each image by employing equations (14) and (15).

4. Experiment and analysis

Our proposed calibration method will be validated by both computer simulation and real calibration experiment. The calibration accuracy with both training and testing data are evaluated by comparing the computed camera parameter values with the simulated or physical values.

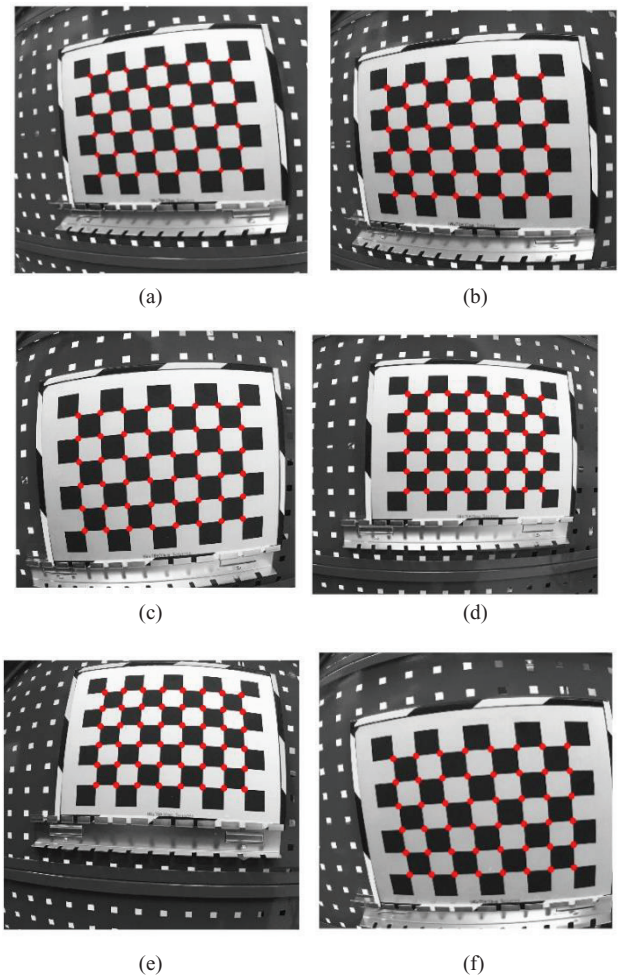

Figure 5. Images captured by the camera. (a)–(f) Show images 1–6, respectively.

4.1. Training data

The number of collinear points directly influences the calibration precision. In terms of the projection optics, if a camera needs to obtain more collinear points in a certain view, a larger target is necessary. We conduct a computer simulation to confirm the validity of our proposed method with different numbers of collinear points. At the meantime, the cross-ratio invariability (CRI) [24] and nonmetric calibration method (NCM) [22], which also decouple the distortion coefficients and camera parameters, are used for comparison.

The resolution of the camera in simulation is 1280×1024 pixels with the principal point at $(u_0,\ v_0) = (640,\ 512)$. The skew factor s is set to zero. The effective focal lengths along the X_m, Y_m orientations in pixels are fx and fy and are 1000 pixels respectively. The radial distortion is simulated with coefficients $k_1 = -0.4\,\mathrm{mm}^{-2}$ and $k_2 = -0.6\,\mathrm{mm}^{-4}$ and tangential distortion coefficients $p_1 = 0.01\,\mathrm{mm}^{-1}$ and $p_2 = 0.0001\,\mathrm{mm}^{-1}$. We simulate five images with different extrinsic parameters (table 1). Considering the existence of image noise, we add Gaussian noise of mean zero and variance of two pixels to each image.

We assume the calibration target is a checkerboard target with $(n \times n)$ corners uniformly distributed. The size of checkerboard is constant. The interval of the adjacent corner is $\frac{200}{n-1}$ mm which decreases along with n increasing. The number of collinear points is n ($n = 5$, 10, 15, 20, 30 40, 50).

Table 2. Comparative results of the intrinsic parameters and distortion coefficients.

Method		Zhang	NCM	Proposed
Calibrated parameters	f_x (pixel)	2313.41	2306	2315.12
	f_y (pixel)	2310.1	2303	2312.18
	u_0 (pixel)	1239.73	1211.58	1225.89
	v_0 (pixel)	1029.57	1018.92	997.33
	$k_1(\mathrm{mm}^{-2})$	−1.884	−1.827	−1.927
	k_2 (mm^{-4})	3.260	5.069	4.643
	p_1 (mm^{-1})	0.0165	0.0169	0.0187
	P_2 (mm^{-1})	0.0004	0.0045	−0.0031

In simulation, the true values of the camera parameters are definite. Hence, we calculate the relative error of the camera parameters to denote the estimated accuracy. The relative error is defined:

$$E_{\mathrm{f}} = \left| \frac{P_{\mathrm{c}} - P_{\mathrm{true}}}{P_{\mathrm{true}}} \right| \times 100\% \tag{16}$$

where P_{c} is the computational camera parameter and P_{true} is its corresponding true value.

The reprojection errors are the distances in pixels between the detected and the reprojected points. We define the mean reprojection error E_{re} for calibration accuracy evaluation as follows:

$$E_{\mathrm{re}} = \frac{1}{nf} \sum_{i=1}^{n} \sum_{j=1}^{f} \left\| \hat{m}_j(i) - \hat{m}_j^r(i) \right\| \tag{17}$$

where $\hat{m}_j^r(i)$ is the reprojection image point coordinate calculated by using equation (1).

The relative error of the distortion coefficients and camera intrinsic parameters is displayed in figure 2. It is noticeable that the number of collinear points has a significant impact on the calibration results.

The comparisons of the mean reprojection error under different numbers of collinear points are shown in figure 3. For each n, five images were performed, and the results shown are the averages. In terms of figure 3, the mean reprojection error of our proposed method is less than that produced by using the NCM and CSI within all numbers. As illustrated by figures 2 and 3, for different numbers of collinear points, particularly when the point number is small, the accuracy obtained from our proposed method is superior to that from the NCM in terms of both the relative error and the reprojection error. Besides this, our approach also works more successfully than CSI, which is very sensitive to the number.

4.2. Real data

To further validate the effectiveness of our proposed method, we also carried out a practical experiment on real data. The result was then compared with that of Zhang's method and the NCM. The camera we used is a piA2400-17gm with

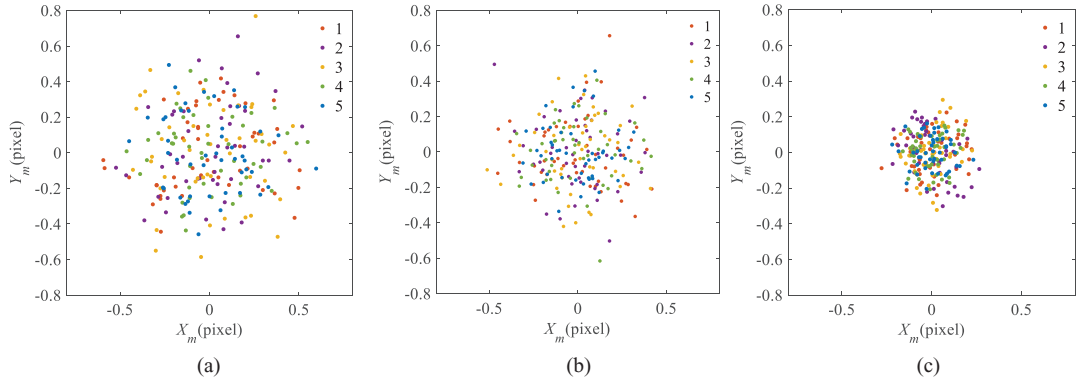

Figure 6. Reprojection errors achieved by the three methods. The point marked as '.' in the figure denotes the reprojection error of the image point. (a) Zhang's method. (b) NCM. (c) Proposed method.

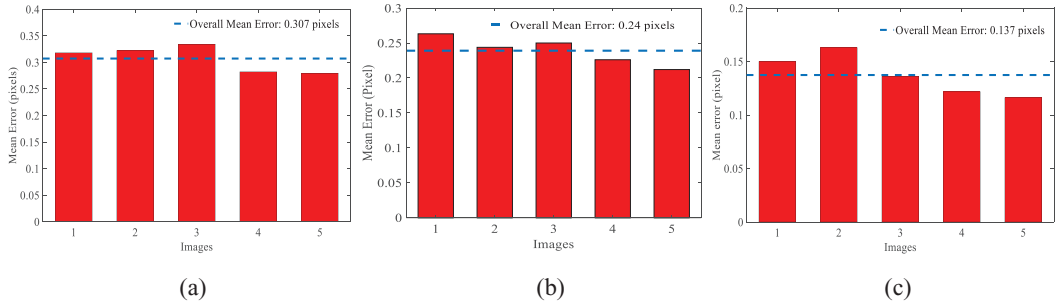

Figure 7. Mean reprojection error of each image achieved by the three methods. (a) Zhang's method. (b) NCM. (b) Proposed method.

resolution 2400 × 2050 pixels. The lens is M1614-MPW2 with a focal length of 16 mm. Because the distortion is most important factor in camera calibration [7, 23], we thus adopt a high distortion lens in our experiment to test our method. Figure 4 shows the calibration experiment system that consists of a camera, a lens, an adjustment mechanism, a computer, and a target.

We use the calibration planar chessboard pattern with 48 corners (8 × 6) uniformly distributed. The minimum point interval is 30 mm in both the horizontal and vertical directions. The manufactural precision of the chessboard is 0.02 mm which is enough to evaluate the camera calibration. Each image includes 48 points and each straight line we used to estimate the lens distortion has 8 or 6 points. It is easy to observe the lens distortion within figure 5.

We randomly take six images from different views and locations, and the calibration procedure is carried out with these images. We compare our proposed method with Zhang's method and the NCM respectively. The calibration results of different methods, including the intrinsic parameters and lens distortion coefficients, are shown in table 2.

The comparison of the reprojection error distributions evaluated by the three methods are displayed in figure 6. Figure 7 shows the mean reprojection error of each image, and intuitively shows the performance of calibration. Both figures 6 and 7 indicate the calibration accuracy of the proposed method is higher than that of Zhang's method and the NCM. The average E_{re} of five images calculated by Zhang's method is 0.307 pixels, 0.240 pixels by the NCM, which are significantly larger than the 0.137 pixels produced by our method.

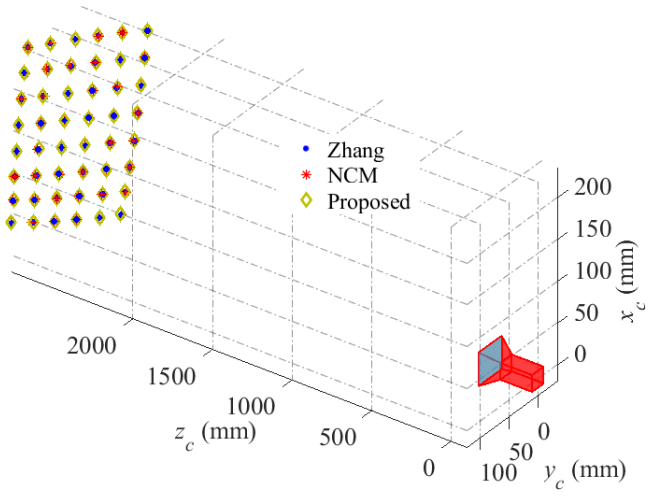

Figure 8. Position of corner points as calculated by using the three methods.

In addition, in order to further validate the calibration method, we apply a measurement validation test to our calibrated camera. As the 3D standard object is too expensive and not available, we utilize the chessboard to replace it. Since five of the six images are used to calibrate the camera to show the performance of the calibration, the unused image is utilized to evaluate the measurement accuracy. We calculate the distance of the corner points according to the calibration parameters of three methods separately.

We define the distance error as below:

$$E_{\text{d}} = |D_{\text{true}} - d| . \tag{18}$$

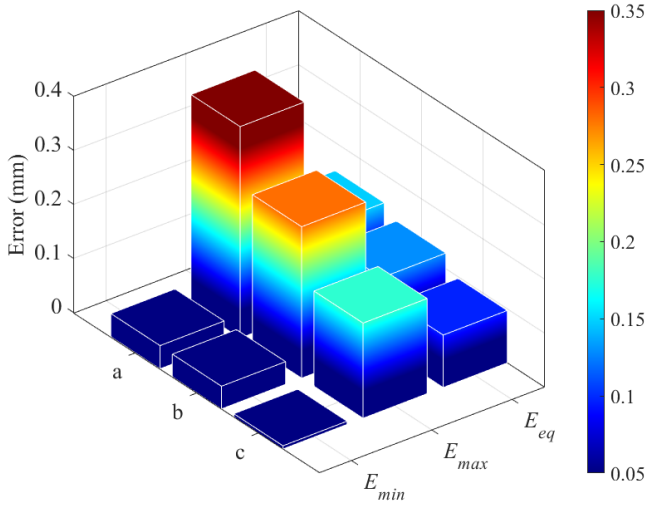

Figure 9. Comparison of distance errors. Note: a represents Zhang's method, b the NCM, and c our proposed method.

Table 3. Comparison of distance errors under different calibration parameters.

	Distance error/E_d (mm)		
Method	E_{min}	E_{max}	E_{eq}
Zhang	0.043	0.391	0.148
NCM	0.041	0.280	0.129
Proposed method	0.006	0.176	0.097

Here D_{true} is the true distance of adjoin feature points, which is equal to 30 mm in this experiment, and the d is the measurement distance.

The maximum distance error E_{max}, the minimum distance error E_{min}, and the mean distance error E_{eq} are defined below:

$$\begin{cases} E_{max} = \max\limits_{1}^{N}(E_d) \\ E_{min} = \min\limits_{1}^{N}(E_d) \\ E_{eq} = \sum\limits_{1}^{N}(E_d) \end{cases}. \tag{19}$$

According to the calibrated parameters by these three methods, we utilize the principle of vision measurement based on the camera model in section 2 to calculate the distance of the adjoin points. The position of the corner points of the sixth image as calculated by using the three methods is shown in figure 8. Based on this, the distance error of the adjoin feature points is determined.

To illustrate the results quantitatively, we draw figure 9 and table 3 based on the distance error results. From both the figure and table, we see that the distance error based on our proposed calibration method is less than that of Zhang's and the NCM. The mean distance error from using Zhang's method is 0.148 mm, and from the NCM is 0.129 mm, which is about two times more than our 0.097 mm. In summary, this supports the notion that the performance of our proposed method is superior to the other referenced methods in the constructed practical measurement process.

5. Conclusion

In this paper, a novel effective vision sensor calibration method using GSC is proposed. This method can be divided into lens distortion coefficient and linear parameter calibration. The GSC model is constructed to obtain the distortion coefficients. The corrected images are used to calculate the linear parameters based on a linear model of the camera. To validate the effectiveness of our proposed method, we have carried out experiments by using both computer simulation and practical experiment. The simulation results show that the calibration performance of our proposed method is superior to that of the NCM and CRI under different numbers of collinear points. The real experiment results also indicate that the average reprojection error calculated by Zhang's method and the NCM is 0.307 and 0.240 pixels, respectively, significantly larger than the 0.137 pixels calculated by our method. Meanwhile, distance error can be used to inspect the measurement precision. The mean distance error using Zhang's method is 0.148 mm, and 0.129 mm using the NCM, nearly two times our result of 0.097 mm. Our proposed calibration method is therefore likely to produce effective and feasible results when practically employed.

Funding

National Science Foundation (NSF) (CNS-1337722); National Institutes of Health (12R1HL124443); Beijing Natural Science Foundation (3172020).

ORCID iDs

Qiyue Wang https://orcid.org/0000-0002-8348-6469

References

[1] Wang Z, Yao Z and Wang Q 2017 Improved scheme of estimating motion blur parameters for image restoration *Digit. Signal Process.* **65** 11–8
[2] Wang Q, Wang Z and Smith T 2016 Radial distortion correction in a vision system *Appl. Opt.* **55** 8876–83
[3] Wang Q, Wang Z, Yao Z, Forrest J and Zhou W 2016 An improved measurement model of binocular vision using geometrical approximation *Meas. Sci. Technol.* **27** 125013
[4] Urban S, Leitloff J and Hinz S 2015 Improved wide-angle, fisheye and omnidirectional camera calibration *ISPRS J. Photogramm. Remote Sens.* **108** 72–9
[5] Ergun B, Kavzoglu T, Colkesen I and Sahin C 2010 Data filtering with support vector machines in geometric camera calibration *Opt. Express* **18** 1927–36
[6] Ricolfe-Viala C, Sanchez-Salmeron A-J and Valera A 2012 Calibration of a trinocular system formed with wide angle lens cameras *Opt. Express* **20** 27691–6
[7] Tsai R 1987 A versatile camera calibration technique for high-accuracy 3D machine vision metrology using off-the-shelf TV cameras and lenses *IEEE J. Robot. Autom.* **3** 323–44
[8] Weng J, Cohen P and Herniou M 1992 Camera calibration with distortion models and accuracy evaluation *IEEE Trans. Pattern Anal. Mach. Intell.* **10** 965–80

[9] Camposeco F, Sattler T and Pollefeys M 2015 Non-parametric structure-based calibration of radially symmetric cameras *Proc. of the IEEE Int. Conf. on Computer Vision* pp 2192–200
[10] Brito J H, Angst R, Koser K and Pollefeys M 2013 Radial distortion self-calibration *Proc. of the IEEE Conf. on Computer Vision and Pattern Recognition* pp 1368–75
[11] Micusik B and Pajdla T 2006 Structure from motion with wide circular field of view cameras *IEEE Trans. Pattern Anal. Mach. Intell.* **28** 1135–49
[12] Hu Y, Chen Q, Feng S, Tao T, Asundi A and Zuo C 2019 A new microscopic telecentric stereo vision system - calibration, rectification, and three-dimensional reconstruction *Opt. Lasers Eng.* **113** 14–22
[13] Heikkila J 2000 Geometric camera calibration using circular control points *IEEE Trans. Pattern Anal. Mach. Intell.* **22** 1066–77
[14] Ricolfe-Viala C and Sánchez-Salmerón A-J 2010 Robust metric calibration of non-linear camera lens distortion *Pattern Recognit.* **43** 1688–99
[15] Bell T, Xu J and Zhang S 2016 Method for out-of-focus camera calibration *Appl. Opt.* **55** 2346–52
[16] Song L M *et al* 2007 High precision camera calibration in vision measurement *Opt. Laser Technol.* **39** 1413–20
[17] Zhang Z 2000 A flexible new technique for camera calibration *IEEE Trans. Pattern Anal. Mach. Intell.* **22** 1130–4
[18] Ji Q and Zhang Y 2001 Camera calibration with genetic algorithms *IEEE Trans. Systems, Man, and Cybernetics-Part A: Syst. Hum.* **31** 120–30
[19] Rahman T and Krouglicof N 2012 An efficient camera calibration technique offering robustness and accuracy over a wide range of lens distortion *IEEE Trans. Image Process.* **21** 626–37
[20] Junejo I N and Foroosh H 2012 Optimizing PTZ camera calibration from two images *Mach. Vis. Appl.* **23** 375–89
[21] Luhmann T, Fraser C and Maas H-G 2016 Sensor modelling and camera calibration for close-range photogrammetry *ISPRS J. Photogramm. Remote Sens.* **115** 37–46
[22] Ahmed M and Farag A 2005 Nonmetric calibration of camera lens distortion: differential methods and robust estimation *IEEE Trans. Image Process.* **14** 1215–30
[23] Zhou F, Cui Y, Gao H and Wang Y 2013 Line-based camera calibration with lens distortion correction from a single image *Opt. Lasers Eng.* **51** 1332–43
[24] Zhang G, He J and Yang X 2003 Calibrating camera radial distortion with cross-ratio invariability *Opt. Laser Technol.* **35** 457–61
[25] Poulin-Girard A-S, Thibault S and Laurendeau D 2016 Influence of camera calibration conditions on the accuracy of 3d reconstruction *Opt. Express* **24** 2678–86
[26] Zhou F *et al* 2017 Calibrating non-central catadioptric vision system using local target reconstruction *Meas. Sci. Technol.* **28** 065009
[27] Hong Y, Ren G and Liu E 2015 Non-iterative method for camera calibration *Opt. Express* **23** 23992–4003